

LCNN: Low-level Feature Embedded CNN for Salient Object Detection

Hongyang Li, *Student Member, IEEE*, Huchuan Lu, *Senior Member, IEEE*, Zhe Lin, *Member, IEEE*, Xiaohui Shen, *Member, IEEE*, and Brian Price, *Member, IEEE*

Abstract—In this paper, we propose a novel deep neural network framework embedded with low-level features (LCNN) for salient object detection in complex images. We utilise the advantage of convolutional neural networks to automatically learn the high-level features that capture the structured information and semantic context in the image. In order to better adapt a CNN model into the saliency task, we redesign the network architecture based on the small-scale datasets. Several low-level features are extracted, which can effectively capture contrast and spatial information in the salient regions, and incorporated to compensate with the learned high-level features at the output of the last fully connected layer. The concatenated feature vector is further fed into a hinge-loss SVM detector in a joint discriminative learning manner and the final saliency score of each region within the bounding box is obtained by the linear combination of the detector’s weights. Experiments on three challenging benchmarks (MSRA-5000, PASCAL-S, ECCSD) demonstrate our algorithm to be effective and superior than most low-level oriented state-of-the-arts in terms of P-R curves, F-measure and mean absolute errors.

Index Terms—Convolutional Neural Networks, Feature Learning, Saliency Detection.

I. INTRODUCTION

HUMANS have the capability to quickly prioritize external visual stimuli and localize interesting regions in a scene. In recent years, visual attention has become an important research problem in both neuroscience and computer vision. One focuses on eye fixation prediction to investigate the mechanism of human visual systems [1] whereas the other concentrates on salient object detection to accurately identify a region of interest [2]. Saliency detection has served as a pre-processing procedure for many vision tasks, such as collages [3], image compression [4], stylized rendering [5], object recognition [6], image retargeting [7], etc.

In this work, we focus on accurate saliency detection. Recently, many low-level features directly extracted from images have been explored. It has been verified that colour contrast is a primary cue for obtaining satisfactory results [8], [5]. Other representations based on the low-level features try to exploit the intrinsic textural difference between the foreground and background, including focusness [9], textual distinctiveness [10], and structure descriptor [11]. They perform well on simple benchmarks, but can still struggle in images of complex scenarios since semantic context hidden in the image cannot be effectively captured by hand-crafted low-level priors (see Figure 1(b)).

Due to the shortcomings of low-level features, several methods have been proposed recently to incorporate high

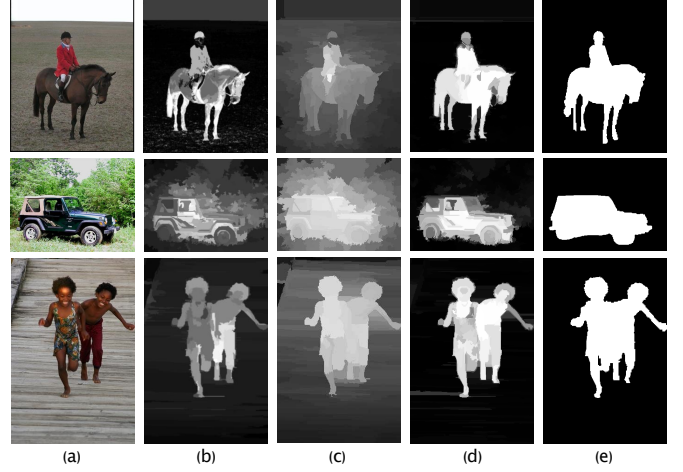


Fig. 1. Saliency detection results by different methods. (a) input images; (b) low-level contrast features by [5]; (c) low-level priors with high-level objectness cues by [12]; (d) our LCNN algorithm, which combines high-level features embedded with low-level priors learned by CNN; (e) ground truth.

level features [13], [9]. One type of such representations that can be employed is the notion of objectness [14], *i.e.*, how likely a given region is an object. For instance, Jiang *et al.* [9] computes the saliency map by combining objectness values of the candidate windows. However, using the existent foreground detectors [15], [16] directly to compute saliency may produce unsatisfying results in complex scenes when the objectness score fails to predict true salient object regions (see Figure 1(c)).

The classic convolutional neural network paradigm [17], [18] has demonstrated superior performance in image classification and detection on the challenging databases with complex background and layout in the images (for instance, PASCAL and ImageNet), which arises from its ability to automatically learn high-level features via a layer-to-layer propagation. This is fundamentally different from previous ‘objectness’ work combining low-level priors. Due to the different application background and the scale of datasets, however, a successful adaption of deep model to saliency detection requires a smaller architecture design, a proper definition of the training examples, some refinement scheme such as a low-level feature embedded network, etc.

In this paper, we formulate a novel deep neural network with low-level feature embedded, namely LCNN, which simultaneously leverages the advantage of CNN to capture the high-

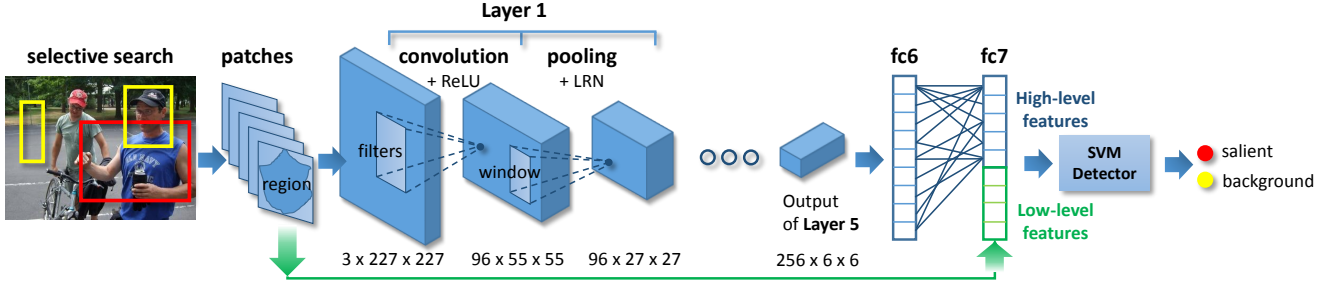


Fig. 2. Pipeline of the low-level feature embedded deep architecture (LCNN).

level features and that of the contrast and spatial information in low-level features. To further facilitate the discriminative characteristics of the network, we combine those extracted features in a joint learning manner via the hinge-loss SVM detector. Figure 1(d) shows the superior advantage of such a deep architecture design, where traditional low-level oriented method [5] or high-level objectness-guided algorithm [12] fails to detect the salient regions in the complex image scenarios (for example, the salient region has similar colour or texture appearance with the background or it is surrounded by the complicated background).

Figure 2 depicts the general pipeline of our method. First, a set of candidate bounding boxes with internal region masks are generated by the selective search method [19]; Next, the warped patches are fed into the deep network to extract high-level features. We make amendments of the classic CNN architecture for adaption to the saliency detection problem; Third, a series of simple and effective low-level descriptors are extracted from the regions within each bounding box; Finally, the concatenated feature vector is fed as input to the discriminative SVM detector and the saliency map is generated from the summation of the detector’s confidence score. The experimental results show that the proposed method achieves superior performance in various evaluation metrics against the state-of-the-art approaches on three challenging benchmarks.

The rest of our paper reviews related works in section II, describes in detail our CNN framework in section III and low-level feature embedded scheme in section IV, verifies the proposed model in section V and concludes the work in section VI. Finally, the results and codes will be shared online upon acceptance.

II. RELATED WORKS

In this section, we discuss the related saliency detection methods and their connection to generic object detection algorithms. In addition, we also briefly review deep neural networks that are closely related to this work.

Saliency estimation methods can be explored from different perspectives. Basically, most works employ a bottom-up approach via low-level features while a few incorporate a top-down solution driven by specific tasks. In the seminal work by Itti *et al.* [20], center-surround differences across multi-scales of image features are computed to detect local conspicuity. Ma and Zhang [21] utilize color contrast in a local

neighborhood as a measure of saliency. In [22], the saliency values are measured by the equilibrium distribution of Markov chains over different feature maps. Achanta *et al.* [2] estimate visual saliency by computing the colour difference between each pixel w.r.t its mean. Histogram-based global contrast and spatial coherence are used in [5] to detect saliency. Liu *et al.* [23] propose a set of features from both local and global views, which are integrated by a conditional random field to generate a saliency map. In [8], two contrast measures based on the uniqueness and spatial distribution of regions are defined for saliency detection. To identify small high contrast regions, [24] propose a multi-layer approach to analyse the saliency cues. A regression model is proposed in [25] to directly map regional feature vectors to saliency scores. Recently, [26] present a background measurement scheme to utilise boundary prior for saliency detection. Liu *et al.* [27] solve saliency detection in a novel partial differential equation manner, where the saliency of certain seeds are propagated until the equilibrium in the image is ensured. In [28], colour contrast in higher dimension space is investigated to diversify the distinctness among superpixels.

Although significant advances have been made, most of the aforementioned methods integrate hand-crafted features heuristically to generate the final saliency map, and do not perform well on challenging benchmarks. In contrast, we devise a deep network based method embedded with simple low-level priors (LCNN) to automatically learn features that disclosure the internal properties of regions and semantic context in complex scenarios.

Generic object detection methods aim at generating the locations of all category independent objects in an image and have attracted growing interest in recent years. Existing techniques propose object candidates by either measuring the objectness of an image window [14], [15] or grouping regions in a bottom-up process [16]. The generated object candidates can significantly reduce the search space of category specific object detectors, which in turn helps other stages for recognition and other tasks. To this end, generic object detection are closely related to salient object detection. In [14], saliency score is utilized as objectness measurement to generate object candidates. [12] use a graphical model to exploit the relationship of objectness and saliency cues for salient object detection. In [29], a random forest model is trained to predict the saliency score of an object candidate.

TABLE I
ARCHITECTURE DETAILS OF THE PROPOSED DEEP NETWORKS. C: CONVOLUTIONAL LAYER; F: FULLY-CONNECTED LAYER; P: POOLING LAYER; R: RECTIFIED LINEAR UNIT (ReLU); N: LOCAL RESPONSE NORMALIZATION (LRN); D: DROPOUT SCHEME; CHANNEL: THE NUMBER OF OUTPUT FEATURE MAPS; PADDING: THE NUMBER OF PIXELS TO ADD TO EACH SIDE OF THE INPUT DURING CONVOLUTION.

Layer	1	2	3	4	5	6	7
Type	C+R+P+N	C+R+P+N	C+R	C+R+P	C+R+P	F+R+D	F+R+D
Input size	227×227	27×27	13×13	13×13	6×6	2×2	$512 + 104$
Channel	96	256	384	384	256	—	—
Filter size	11×11	5×5	3×3	3×3	3×3	—	—
Filter stride	4	—	—	—	—	—	—
Padding	—	2	1	1	1	—	—
Pooling size	3×3	3×3	—	3×3	3×3	—	—
Pooling stride	2	2	—	2	3	—	—

In this work, we utilise the selective search method [19] to generate a series of potential foreground bounding boxes as a preliminary preparation for the inputs of the deep network.

Deep neural networks have achieved state-of-the-art results in image classification [30], [31], object detection [32], [33] and scene parsing [34], [35]. The success stems from the expressibility and capacity of deep architectures that facilitates learning complex features and models to account for interacted relationships directly from training examples. Since DNNs mainly take image patches as inputs, they tend to fail in capturing long range label dependencies for scene parsing as well as saliency detection. To address this issue, [35] use a recurrent convolutional neural network to consider large contexts. In [34], a DNN is applied in a multi-scale manner to learn hierarchical feature representations for scene labeling. We propose a revised CNN pipeline with low-level feature embedded to consider the label (region) dependencies based on contrast and spatial descriptors, which is of vital importance in the saliency detection task.

III. CNN BASED SALIENCY DETECTION

The motivation of applying CNN to saliency detection is that the network can automatically learn structured and representative features via a layer-to-layer hierarchical propagation scheme, where we do not have to design complicated hand-crafted features. The key points to make CNN work for saliency are (a): redesigned network architecture, which means, unlike [18] on the ImageNet [36], too many layers or parameters will burden the computation in a relatively small-scale saliency dataset; (b): proper definition of positive training examples, that is to say, considering the size of various (maybe multiple) salient object(s), how to define a positive region within the box compared with the ground truth; (c) how to add some ‘refinement’ scheme at the output of the last layer to better fit in the accurate saliency detection. Through section III-A to III-C, we will disclosure the solutions of the aforementioned issues respectively.

A. Network architecture

The proposed CNN consists of seven layers, with five convolutional layers and two fully connected layers. Each

layer contains learnable parameters and consists of a linear transformation followed by a nonlinear mapping, which is implemented by rectified linear units (ReLUs) [17] to accelerate the training process. Local response normalization (LRN) is applied to the first two layers to help generalization. Max pooling is applied to all convolutional layers except for the third layer to ensure translational invariance. The dropout scheme is utilized after the first and the second fully connected layers to avoid overfitting. The network takes as input a warped RGB image patch of size 227×227 , and outputs a 512-dimension feature vector for the SVM detector¹. The detailed architecture of the network is shown in Table I.

To generate the squared patches both for training and test, we first use the selective search method [19] to propose around 2,000 boxes, each of which also includes the region mask segmented in different color spaces by [37]. Note that we take a preliminary selection scheme to filter out small boxes or those whose region mask accounts for little area w.r.t. the whole box. Then we warp all pixels in the tight bounding box around it to the required size. Prior to warping, we pad the box to include more local context as does [18].

B. Network training

Training data. To label the training boxes, we mainly consider the intersection between the bounding box and the ground truth mask. A box B is considered as positive sample if it sufficiently overlaps with the ground truth region G : $|B \cap G| \geq 0.7 \times \max(|B|, |G|)$; similarly, a box is labeled as negative sample if $|B \cap G| \leq 0.3 \times \max(|B|, |G|)$. The remaining samples labeled as neither positive nor negative are not used. Following [17], we do not pre-process the training samples, except for subtracting the mean values over the training set from each pixel. The labelling criteria and the process of patch generation are illustrated in Figure 3(a)-(b).

Cost function. Given the training box set $\{B_i\}^N$ and the corresponding label set $\{y_i\}^N$, we use the softmax loss with

¹ In the original CNN framework, layer 7 outputs the same feature length (1024-dimension) as layer 6 does. In order to better balance between high-level and low-level features, we reduce the output number of layer 7 to 512-dimension. Note that in latter experiments without the low-level feature embedded architecture, layer 7 still outputs a 1024-dimension feature vector.

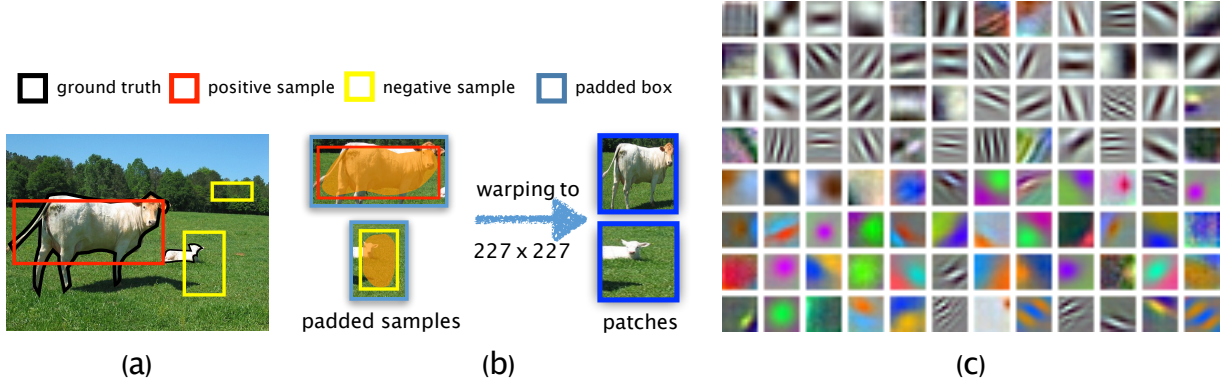


Fig. 3. (a) Illustration of labelling; (b) Generation of patches. Note that the orange region inside each padded sample is the ‘cell unit’ in our task, which means we use it to extract low-level features and compute saliency; (c) Visualization of the 96 learned filters in the first layer.

weight decay as the cost function:

$$L(\theta) = -\frac{1}{m} \sum_{i=1}^m \sum_{j=0}^1 \delta(y_i, j) \log P(y_i = j | \theta) + \lambda \sum_{k=1}^7 \|\mathbf{W}_k\| \quad (1)$$

where θ denotes the learnable parameters set of CNN including the weights and bias of all layers; δ is the indicator function; $P(y_i = j | \theta)$ is the label probability of the i -th training example predicted by CNN; λ is the weight decay parameter; and \mathbf{W}_k indicates the weight of the k -th layer. CNN is trained using stochastic gradient descent with a batch size of $m = 256$, momentum of 0.9, and weight decay of 0.0005. The learning rate is initially set to 0.01 and is decreased by a factor of 0.1 when the cost is stabilized. Figure 3(c) illustrates the learned convolutional filters in the first layer, which capture color, contrast, edge and pattern information of the local neighborhoods.

C. CNN for Saliency detection

During the test stage, we feed the trained network with padded and warped patches and predict the saliency score of each bounding box using the probability $P(y = 1 | \theta)$. A primitive saliency map is obtained by summing up the saliency scores of all the candidate regions within the proposed bounding boxes. Figure 4(b) shows the result of directly applying CNN’s last layer as the saliency detector to generate saliency maps, which is denoted as the baseline model. However, as are shown in later experiment (section V-B) and [18], such a straightforward strategy may suffer from the definition of positive examples used in training the network, which does not emphasise the precise salient localisation within the bounding boxes.

To this end, we introduce a discriminative learning method using the l_1 hinge-loss SVM to further classify the extracted high-level features (*i.e.*, the output of layer 7). The objective function is formulated as:

$$\arg \min_{\mathbf{w}} \frac{1}{2} \|\mathbf{w}\|^2 + C \sum_{i=1}^N \max(0, 1 - y_i \mathbf{w}^T \mathbf{x}_i) \quad (2)$$

where \mathbf{w} is the weights of the SVM detector and C the penalty coefficient. Here we set $C = 0.001$ to ensure the computation efficiency. The revised saliency score of each bounding box or internal region is calculated as $\mathbf{w} \cdot \mathbf{x}^7 + \mathbf{b}$, where \mathbf{w}, \mathbf{b} represent the weights and biases of the detector and \mathbf{x}^7 being the output feature vector of the fc7 layer. Figure 4(c) depicts the visual enhancement of the saliency maps after enforcing a SVM mechanism, which can discriminatively choose representative high-level features to determine saliency for the region.

So far, the CNN framework with a SVM detector predicts saliency values based solely on the automatic learned high-level features, which can include high-level semantic context in the image via the box padding and a layer-to-layer propagation scheme. We find by adding some simple low-level priors, such as contrast or geometric information, the CNN framework could obtain much more enhanced results.

IV. LCNN: LOW-LEVEL FEATURE EMBEDDED CNN

The motivation why high-level feature from CNN alone is not enough can be explained as follows. The CNN-based prediction determines saliency solely based on how a particular sub-region looks like an object bounding box; the low-level saliency methods are typically cued on contrast or spatial cues from the global context, which is another valuable information missing in the somewhat ‘local’ CNN prediction. In this section, we propose a small, and yet effective, set of simple low-level features to compensate with those high-level features in a joint learning spirit. Different from [25] where too many low-level features are proved to be redundant [38], we use the most common priors, such as colour contrast and spatial properties. To enlarge the feature space diversity, we also explore the texture information in the image by extracting LBP feature [39] and LM filter banks [40].

A. Exploring low-level features

The proposed 104-dimensional low-level features covers a wide diversity from the colour and texture contrast of a region to the spatial properties of a bounding box. First, given a region R within the bounding box generated by the selective

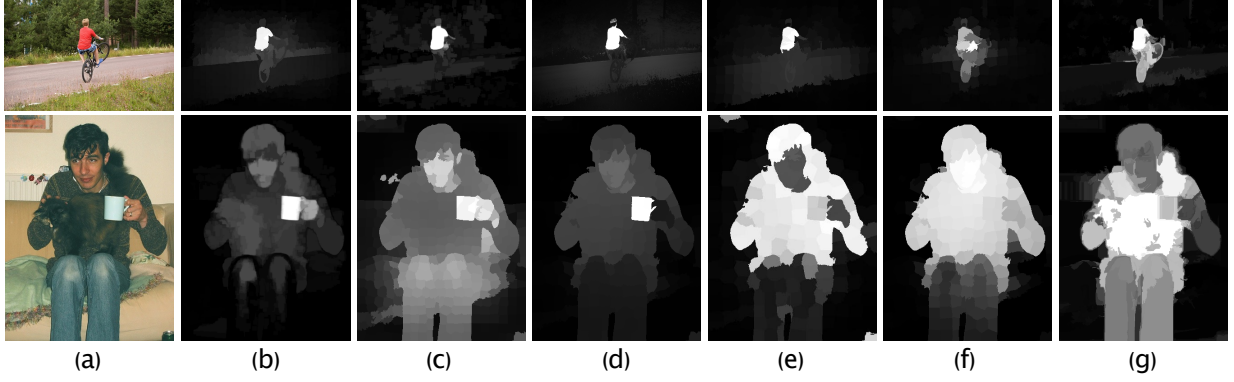


Fig. 4. Resultant saliency maps of different architecture design. (a) input image; (b) baseline model; (c) CNN with SVM detector; (d) CNN with spatial descriptors alone; (e) CNN with contrast descriptors alone; (f) CNN with low-level features (contrast and spatial descriptors together); (g) the proposed LCNN.

search method and using the RGB colour space as an example, we compute its RGB histogram \mathbf{h}_R^{RGB} , average RGB values \mathbf{a}_R^{RGB} and RGB color variance var_R^{RGB} over all the pixels in the candidate region. Then, in order to characterize the texture feature of the region, we calculate the max response histogram of LM filters \mathbf{h}_R^{LM} , the histogram of LBP feature \mathbf{h}_R^{LBP} , the absolute response of LM filters \mathbf{r}_R , as well as the variance of the LBP feature var_R^{LBP} and the LM filters var_R^r . Furthermore, we define the border regions of 20 pixels width in four directions of the image as boundary regions² and compute the measurements \mathbf{h}_B^{CS} , \mathbf{h}_B^{TX} , \mathbf{a}_B^{CS} , \mathbf{r}_B in a similarly way as defined above. Also we consider the colour histogram \mathbf{h}_I^{CS} of the entire image in three colour spaces. Here CS denotes the three colour spaces and TX represents the two texture features extracted by LBP and LM.

Equipped with the aforementioned definitions and notations, we define a series set of low-level features. For the contrast descriptors, we introduce the boundary colour contrast by the chi-square distance $\chi^2(\mathbf{h}_R^{RGB}, \mathbf{h}_B^{RGB})$ between the RGB histograms of the candidate region and the four boundary regions, and the Euclidean distance $d(\mathbf{a}_R^{RGB}, \mathbf{a}_B^{RGB})$ between their mean RGB values. The rest of the colour or texture contrast between the region and the boundary regions, or the entire image are computed similarly. For the spatial descriptors, we not only consider the geometric information of a bounding box, such as the aspect ratio, height/width and centroid coordinates, but also extract the internal colour and texture variance of the candidate region. Note that all the geometric features are normalised w.r.t. the image size. Finally, all the low-level features are summarised in Table II.

B. LCNN for saliency detection

We concatenate the low-level feature vector proposed above with the high-level feature vector generated from layer 7 and use them as input of the SVM detector (see Figure 2). The

² Since the boundary regions in different directions may have different appearance, we compute their measurements separately. For notation convenience, we denote the feature vectors of the boundary regions in each direction with a uniform subscript B .

revised architecture, namely the low-level feature embedded CNN (LCNN), archives better performance than previous schemes. Note that prior to feeding the concatenated feature into the SVM detector, we pre-process the data by subtracting the mean and dividing the standard deviation of the feature elements. The final saliency map follows a similar pipeline as stated in section III-C and we refine the map on a pixel-wise level using the manifold ranking smoothing [7].

Figure 4(d)-(f) illustrates the different effects of low-level features. We can see that the contrast descriptors (row e) play a more important role than the spatial descriptors (row d) as the former considers the appearance distinction between the region and its surroundings. A combination of the low-level features into the CNN framework (row f) can effectively facilitate the accuracy of saliency detection since the low-level priors can catch up the distinctness between the salient regions and the image boundary (usually indicating the background in most cases.). Furthermore, as Figure 4(g) suggests, our final scheme (LCNN), which includes the SVM detector based on the low-level feature embedded deep network, can take advantage of both low-level priors and discriminative learning detector. Note that the bicycle and the person's legs are effectively detected in such a framework whereas previous schemes fail to detection them in some way. Figure 5 in section V-B proves our architecture design in a quantitative manner.

V. EXPERIMENTAL RESULTS

In this section, we first describe in details the experiment settings on datasets, evaluation metrics and training environment (V-A); then the ablation studies are conducted to verify each architecture strategy (V-B); finally we compare the proposed algorithm with the current state-of-the-arts both in a quantitative and qualitative manner (V-C).

A. Setup

The experiments are conducted on three benchmarks: MSRA-5000 [23], ECCSD [24] and PASCAL-S [29]. The MSRA-5000 dataset is widely used for saliency detection and covers a large variety of image contents. Most of the

TABLE II

THE DETAILED DESCRIPTION OF LOW-LEVEL FEATURES. \mathbf{R} DENOTES THE ABSOLUTE RESPONSE OF LM FILTERS.
 $d(\mathbf{A}_1, \mathbf{A}_2) = (|a_{11} - a_{21}|, \dots, |a_{1k} - a_{2k}|)$, WHERE k IS THE FEATURE DIMENSION OF VECTOR \mathbf{A}_1 AND \mathbf{A}_2 ; $\chi^2(\mathbf{H}_1, \mathbf{H}_2) = \sum_{i=1}^b \frac{2(h_{1i} - h_{2i})^2}{h_{1i} + h_{2i}}$ WITH b BEING THE NUMBER OF HISTOGRAM BINS.

Contrast Descriptors (color and texture)				Spatial/Property Descriptors			
Notation	Definition	Notation	Definition	Notation	Definition	Notation	Definition
$c_1 - c_4$	$\chi^2(\mathbf{h}_R^{RGB}, \mathbf{h}_B^{RGB})$	$c_{16} - c_{27}$	$d(\mathbf{a}_R^{RGB}, \mathbf{a}_B^{RGB})$	$p_1 - p_2$	centroid coordinates	$p_{22} - p_{24}$	var_R^{RGB}
$c_5 - c_8$	$\chi^2(\mathbf{h}_R^{Lab}, \mathbf{h}_B^{Lab})$	$c_{28} - c_{39}$	$d(\mathbf{a}_R^{Lab}, \mathbf{a}_B^{Lab})$	p_3	box aspect ratio	$p_{25} - p_{27}$	var_R^{Lab}
$c_9 - c_{12}$	$\chi^2(\mathbf{h}_R^{HSV}, \mathbf{h}_B^{HSV})$	$c_{40} - c_{51}$	$d(\mathbf{a}_R^{HSV}, \mathbf{a}_B^{HSV})$	p_4	box width	$p_{27} - p_{30}$	var_R^{HSV}
c_{13}	$\chi^2(\mathbf{h}_R^{RGB}, \mathbf{h}_I^{RGB})$	$c_{52} - c_{55}$	$\chi^2(\mathbf{h}_R^{LBP}, \mathbf{h}_B^{LBP})$	p_5	box height		
c_{14}	$\chi^2(\mathbf{h}_R^{Lab}, \mathbf{h}_I^{Lab})$	$c_{56} - c_{59}$	$\chi^2(\mathbf{h}_R^{LM}, \mathbf{h}_B^{LM})$	p_6	var_R^{LBP}		
c_{15}	$\chi^2(\mathbf{h}_R^{HSV}, \mathbf{h}_I^{HSV})$	$c_{60} - c_{74}$	$d(\mathbf{r}_R, \mathbf{r}_B)$	$p_7 - p_{21}$	var_R^r		

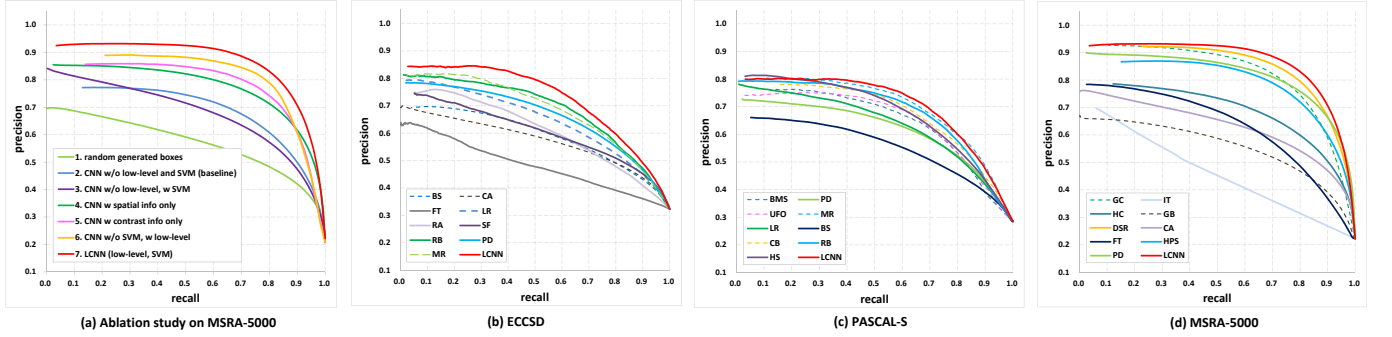


Fig. 5. Ablation study on MSRA-5000 test dataset and quantitative comparison to previous methods on three benchmarks.

images include only one salient object with high contrast to the background. The ECCSD dataset consists of 1000 images with complex scenes from the Internet and is more challenging. The newly released PASCAL-S dataset descends from the validation set of the PASCAL VOC 2012 segmentation challenge. This dataset includes 850 natural images with multiple complex objects and cluttered backgrounds. The PASCAL-S dataset is arguably one of the most challenging saliency datasets without various design biases (e.g., center bias and color contrast bias). All the datasets is bundled with pixel-wise ground truth annotations.

We evaluate the performance using precision-recall (PR) curves, F-measure and mean absolute error (MAE). The precision and recall of a saliency map are computed by segmenting the map with a threshold, and comparing the resultant binary map with the ground truth. The PR curves demonstrate the mean precision and recall of different saliency maps at various thresholds. The F-measure is defined as:

$$F_\beta = \frac{(1 + \beta^2) Precision \times Recall}{\beta^2 Precision + Recall} \quad (3)$$

where *Precision* and *Recall* are computed using twice the mean saliency value of saliency maps as the threshold, and β^2 is set to 0.3. The MAE is the average per-pixel difference between saliency maps S and the ground truth GT :

$$MAE = \frac{1}{W \times H} \sum_{x=1}^W \sum_{y=1}^H |S(x, y) - GT(x, y)|. \quad (4)$$

where W, H denotes the width and height of the saliency map, respectively. The metric takes the true negative saliency assignments into account whereas the precision and recall only favour the successfully assigned saliency to the salient pixels [41].

Since the MSRA-5000 dataset covers various scenarios and the PASCAL-S dataset contains images with complex structures, we randomly choose 2500 images from the MSRA-5000 dataset and 400 images from the PASCAL-S dataset to train the network. The remaining images are used for tests. Both horizontal refection and rescaling ($\pm 5\%$) are applied to all the training images to augment the training dataset. The training process is implemented using the Caffe framework [42] and initialised with default parameter setting as suggested in [17]. We train the network for roughly 80 epochs through the training set of 1.3 million samples, which takes three weeks on a NVIDIA GTX 760 4GB GPU.

B. Ablation studies

Figure 5(a) investigates the performance distinction of different architecture designs on MSRA-5000 test dataset in a quantitative manner. Note that without a preliminary selective search scheme (line 1), the network suffers from severe insufficient positive samples during training and lacks a proper foreground ‘guidance’ to predict saliency during test stage.

³ Note that we round the values to 2 decimal digits.

TABLE III

QUANTITATIVE RESULTS USING F-MEASURE (HIGHER IS BETTER) AND MAE (LOWER IS BETTER). THE BEST THREE RESULTS ARE HIGHLIGHTED IN RED, BLUE AND GREEN, RESPECTIVELY.

Dataset	Metric	GC	HS	MR	PD	SVO	UFO	HPS	RB	HCT	BMS	DSR	LCNN
ECCSD	F-measure	0.56 ³	0.63	0.70	0.58	0.24	0.64	0.60	0.67	0.64	0.62	0.61	0.71
	MAE	0.22	0.23	0.19	0.25	0.41	0.21	0.25	0.18	0.20	0.22	0.24	0.16
PASCAL-S	F-measure	0.49	0.54	0.60	0.53	0.27	0.55	0.52	0.61	0.54	0.58	0.57	0.65
	MAE	0.25	0.25	0.21	0.24	0.37	0.23	0.26	0.19	0.23	0.21	0.24	0.16
MSRA-5000	F-measure	0.70	0.77	0.79	0.71	0.30	0.77	0.71	0.78	0.77	0.75	0.76	0.79
	MAE	0.15	0.16	0.13	0.20	0.36	0.15	0.21	0.11	0.14	0.16	0.14	0.12

Also the rough score summation of bounding boxes can only generate fuzzy and blurry saliency maps, which is incapable of conducting a precise salient object detection task. The baseline model (line 2) takes a primitive architecture of Table I without the final regression scheme and the introduction of low-level features. We can see the performance improves slightly after the incorporation of the SVM detector (line 3), particularly in the range of low recall values. Line 4-6 investigates the different effects of low-level features. We find that the contrast descriptors (line 5) plays a more important role to facilitate the saliency accuracy that does the spatial descriptors (line 4); and a combination of both contrast and spatial features (line 6) can effectively enhance the result. Finally, the SVM detector can discriminatively classify the extracted features into the foreground and the background, thus formulating our final version of the low-level feature embedded CNN architecture (line 7).

C. Performance comparison

We compare the proposed method (LCNN) with the traditional low-level oriented algorithms as well as the newly published state-of-the-arts: IT [20], GB [22], FT [2], CA [3], RA [43], BS [44], LR [13], SVO [12], CB [45], SF [8], HC [5], PD [46], MR [47], HS [24], BMS[48], UFO [9], DSR [49], HPS [7], GC [41], RB [26], HCT [28]. We use either the implementations or the saliency maps provided by the authors for pair comparison.

Our method performs favourably against the state-of-the-arts on three benchmarks in terms of P-R curves (Figure 5), F-measure as well as MAE scores (Table III). We achieve the highest F-measure value of 0.712, 0.648 and the lowest MAE of 0.161, 0.164 on the ECCSD and PASCAL-S dataset, respectively. And the performance on the MSRA-5000 dataset is very close to the best method [47]. Figure 6 reports the visual comparison of different saliency maps. Our algorithm can effectively catch key colour or structure information in complex image scenarios by both learning low-level features and high-level semantic context.

VI. CONCLUSIONS

In this paper, we address the salient object detection problem by learning the high-level features via deep convolutional

neural networks and incorporating the low-level features into the deep model to enhance the saliency accuracy. To further catch the discriminant semantic context in the complex image scenarios, we introduce a hinge-loss SVM detector to better distinguish the salient region(s) within each bounding box. Experimental results show that our algorithm achieves superior performance against the state-of-the-arts on three benchmarks. A straightforward extension to our method is to jointly learn global and local saliency context through a novel neural network architecture instead of relying on hand-crafted low-level features, which will be left as our future work.

REFERENCES

- [1] T. Judd, K. Ehinger, F. Durand, and A. Torralba, "Learning to predict where humans look," in *ICCV*, 2009. 1
- [2] R. Achanta, S. Hemami, F. Estrada, and S. Süsstrunk, "Frequency-tuned salient region detection," in *CVPR*, 2009. 1, 2, 7
- [3] S. Goferman, L. Zelnik-Manor, and A. Tal, "Context-aware saliency detection," in *CVPR*, 2010. 1, 7
- [4] L. Itti, "Automatic foveation for video compression using a neurobiological model of visual attention," *IEEE Trans. Image Proc.*, vol. 13, no. 10, pp. 1304–1318, Oct 2004. 1
- [5] M.-M. Cheng, G.-X. Zhang, N. J. Mitra, X. Huang, and S.-M. Hu, "Global contrast based salient region detection," in *CVPR*, 2011. 1, 2, 7
- [6] U. Rutishauser, D. Walther, C. Koch, and P. Perona, "Is bottom-up attention useful for object recognition?" in *CVPR*, 2004. 1
- [7] X. Li, Y. Li, C. Shen, A. Dick, and A. Hengel, "Contextual hypergraph modeling for salient object detection," in *ICCV*, 2013. 1, 5, 7
- [8] F. Perazzi, P. Krähenbühl, Y. Pritch, and A. Hornung, "Saliency filters: Contrast based filtering for salient region detection," in *CVPR*, 2012. 1, 2, 7
- [9] P. Jiang, H. Ling, J. Yu, and J. Peng, "Salient region detection by UFO: Uniqueness, Focusness and Objectness," in *ICCV*, 2013. 1, 7
- [10] C. Scharfenberger, A. Wong, K. Fergani, J. S. Zelek, and D. A. Clausi, "Statistical textural distinctiveness for salient region detection in natural images," in *CVPR*, 2013. 1
- [11] K. Shi, K. Wang, J. Lu, and L. Lin, "PISA: Pixelwise image saliency by aggregating complementary appearance contrast measures with spatial priors," in *CVPR*, 2013. 1
- [12] K.-Y. Chang, T.-L. Liu, H.-T. Chen, and S.-H. Lai, "Fusing generic objectness and visual saliency for salient object detection," in *ICCV*, 2011. 1, 2, 7
- [13] X. Shen and Y. Wu, "A unified approach to salient object detection via low rank matrix recovery," in *CVPR*, 2012. 1, 7
- [14] B. Alexe, T. Deselaers, and V. Ferrari, "Measuring the objectness of image windows," *IEEE Transactions on Pattern Analysis and Machine Intelligence*, vol. 34, no. 11, pp. 2189–2202, 2012. 1, 2
- [15] M.-M. Cheng, Z. Zhang, W.-Y. Lin, and P. H. S. Torr, "BING: Binarized normed gradients for objectness estimation at 300fps," in *CVPR*, 2014. 1, 2
- [16] P. Krähenbühl and V. Koltun, "Geodesic object proposals," in *ECCV*, 2014. 1, 2

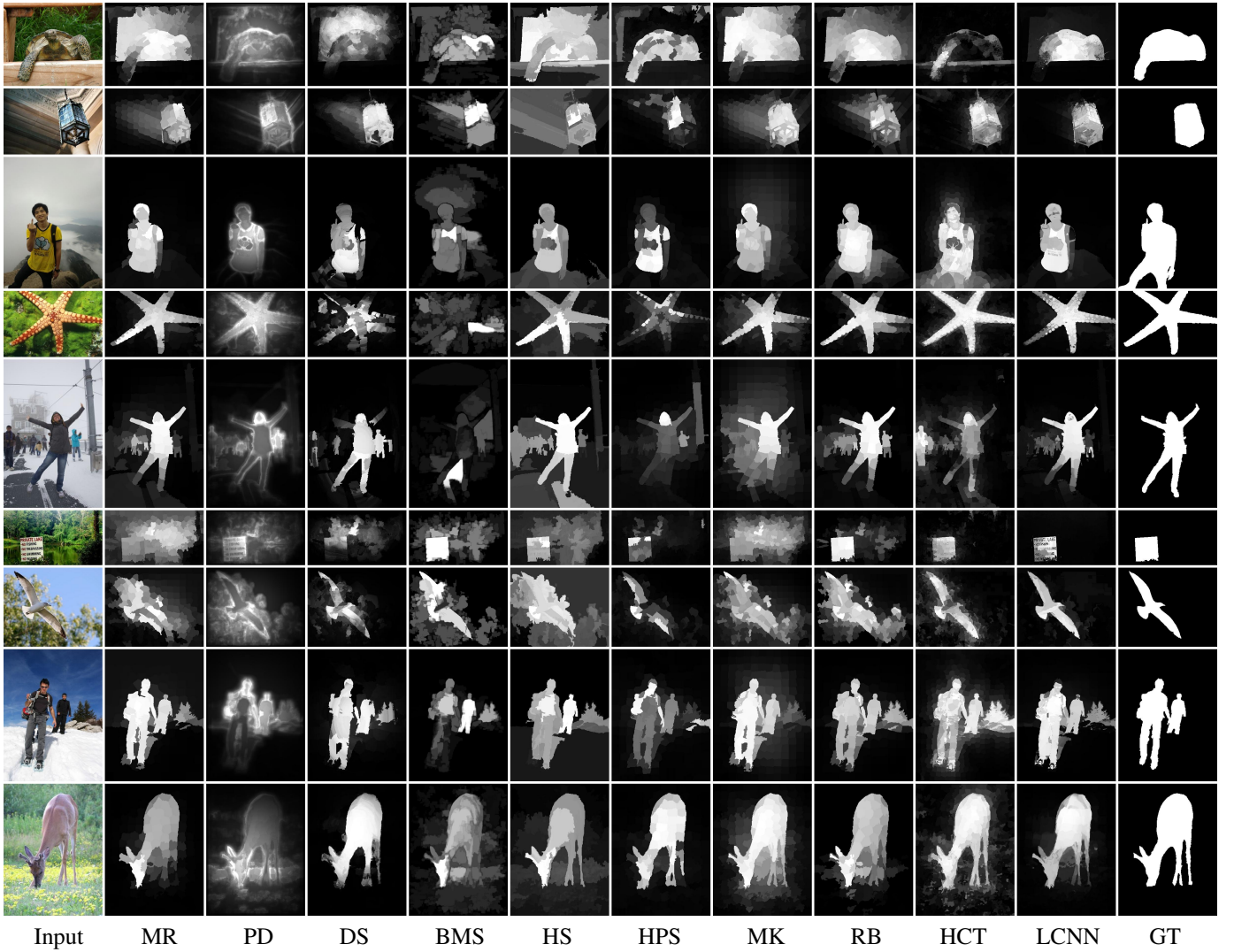


Fig. 6. Visual comparison of the newest methods published in 2013 and 2014, our algorithm (LCNN) and ground truth (GT).

- [17] A. Krizhevsky, I. Sutskever, and G. E. Hinton, “ImageNet classification with deep convolutional neural networks,” in *NIPS*, 2012, pp. 1097–1105. [1](#), [3](#), [6](#)
- [18] R. Girshick, J. Donahue, T. Darrell, and J. Malik, “Rich feature hierarchies for accurate object detection and semantic segmentation,” in *CVPR*, 2014. [1](#), [3](#), [4](#)
- [19] J. Uijlings, K. van de Sande, T. Gevers, and A. Smeulders, “Selective search for object recognition,” *International Journal of Computer Vision*, 2013. [2](#), [3](#)
- [20] L. Itti, C. Koch, and E. Niebur, “A model of saliency-based visual attention for rapid scene analysis,” *IEEE Trans. PAMI*, vol. 20, pp. 1254–1259, 1998. [2](#), [7](#)
- [21] Y.-F. Ma and H.-J. Zhang, “Contrast-based image attention analysis by using fuzzy growing,” 2003. [2](#)
- [22] J. Harel, C. Koch, and P. Perona, “Graph-based visual saliency,” in *NIPS*, 2007. [2](#), [7](#)
- [23] T. Liu, Z. Yuan, J. Sun, J. Wang, N. Zheng, X. Tang, and H. Shum, “Learning to detect a salient object,” *IEEE Trans. PAMI*, vol. 33, 2011. [2](#), [5](#)
- [24] Q. Yan, L. Xu, J. Shi, and J. Jia, “Hierarchical saliency detection,” in *CVPR*, 2013. [2](#), [5](#), [7](#)
- [25] H. Jiang, J. Wang, Z. Yuan, Y. Wu, N. Zheng, and S. Li, “Salient object detection: A discriminative regional feature integration approach,” in *CVPR*, 2013. [2](#), [4](#)
- [26] W. Zhu, S. Liang, Y. Wei, and J. Sun, “Saliency optimization from robust background detection,” in *CVPR*, 2014. [2](#), [7](#)
- [27] R. Liu, J. Cao, Z. Lin, and S. Shan, “Adaptive partial differential equation learning for visual saliency detection,” in *CVPR*, 2014. [2](#)
- [28] J. Kim, D. Han, Y.-W. Tai, and J. Kim, “Salient region detection via high-dimensional color transform,” in *CVPR*, 2014. [2](#), [7](#)
- [29] Y. Li, X. Hou, C. Koch, J. M. Rehg, and A. L. Yuille, “The secrets of salient object segmentation,” in *CVPR*, 2014. [2](#), [5](#)
- [30] J. Donahue, Y. Jia, O. Vinyals, J. Hoffman, N. Zhang, E. Tzeng, and T. Darrell, “DeCAF: A deep convolutional activation feature for generic visual recognition,” 2014. [3](#)
- [31] C. Szegedy, A. Toshev, and D. Erhan, “Deep neural networks for object detection,” in *NIPS*, C. Burges, L. Bottou, M. Welling, Z. Ghahramani, and K. Weinberger, Eds., 2013. [3](#)
- [32] C. Szegedy, W. Liu, Y. Jia, P. Sermanet, S. Reed, D. Anguelov, D. Erhan, V. Vanhoucke, and A. Rabinovich, “Going deeper with convolutions,” *arXiv preprint arXiv:1409.4842*, 2014. [3](#)
- [33] B. Hariharan, P. Arbeláez, R. Girshick, and J. Malik, “Simultaneous detection and segmentation,” in *ECCV*, 2014. [3](#)
- [34] C. Farabet, C. Couprie, L. Najman, and Y. LeCun, “Learning hierarchical features for scene labeling,” *IEEE Transactions on Pattern Analysis and Machine Intelligence*, August 2013. [3](#)
- [35] P. H. O. Pinheiro and R. Collobert, “Recurrent convolutional neural networks for scene labeling,” in *Proceedings of the 31st International Conference on Machine Learning (ICML)*, 2014. [3](#)
- [36] J. Deng, W. Dong, R. Socher, L.-J. Li, K. Li, and L. Fei-Fei, “ImageNet: A large-scale hierarchical image database,” in *CVPR*, 2009, pp. 248–255. [3](#)

- [37] P. F. Felzenszwalb and D. P. Huttenlocher, "Efficient graph-based image segmentation," *International Journal of Computer Vision*, vol. 59, p. 2004, 2004. 3
- [38] H. Jiang, Z. Yuan, M. Cheng, Y. Gong, N. Zheng, and J. Wang, "Salient object detection: A discriminative regional feature integration approach," *CoRR*, vol. abs/1410.5926, 2014. [Online]. Available: <http://arxiv.org/abs/1410.5926> 4
- [39] M. Heikkilä, M. Pietikäinen, and C. Schmid, "Description of interest regions with local binary patterns," *Pattern recognition*, vol. 42, no. 3, pp. 425–436, 2009. 4
- [40] T. Leung and J. Malik, "Representing and recognizing the visual appearance of materials using three-dimensional textons," *International Journal of Computer Vision*, vol. 43, no. 1, pp. 29–44, 2001. 4
- [41] M.-M. Cheng, J. Warrell, W.-Y. Lin, S. Zheng, V. Vineet, and N. Crook, "Efficient salient region detection with soft image abstraction," in *ICCV*, 2013. 6, 7
- [42] Y. Jia, E. Shelhamer, J. Donahue, S. Karayev, J. Long, R. Girshick, S. Guadarrama, and T. Darrell, "Caffe: Convolutional architecture for fast feature embedding," *arXiv preprint arXiv:1408.5093*, 2014. 6
- [43] E. Rahtu, J. Kannala, M. Salo, and J. Heikkilä, "Segmenting salient objects from images and videos," in *ECCV*, 2010. 7
- [44] Y. Xie and H. Lu, "Visual saliency detection based on Bayesian model," in *ICIP*, 2011. 7
- [45] H. Jiang, J. Wang, Z. Yuan, T. Liu, N. Zheng, and S. Li, "Automatic salient object segmentation based on context and shape prior," in *BMVC*, 2011. 7
- [46] R. Margolin, A. Tal, and L. Zelnik-Manor, "What makes a patch distinct?" in *CVPR*, 2013. 7
- [47] C. Yang, L. Zhang, H. Lu, X. Ruan, and M.-H. Yang, "Saliency detection via graph-based manifold ranking," in *CVPR*, 2013. 7
- [48] J. Zhang and S. Sclaroff, "Saliency detection: A boolean map approach," in *ICCV*, 2013. 7
- [49] X. Li, H. Lu, L. Zhang, X. Ruan, and M.-H. Yang, "Saliency detection via dense and sparse reconstruction," in *ICCV*, 2013. 7